ATMOSPHERIC ENVIRONMENT: X 11 (2021) 100119

Contents lists available at ScienceDirect

Atmospheric Environment: X

journal homepage: www.journals.elsevier.com/atmospheric-environment-x

The impact of temporal variability in prior emissions on the optimization of urban anthropogenic emissions of CO_2, CH_4 and CO using in-situ observations

Ingrid Super *, Stijn N.C. Dellaert, Janot P. Tokaya, Martijn Schaap

Department of Climate, Air and Sustainability, TNO, P.O. Box 80015, 3508, TA Utrecht, Netherlands

ARTICLE INFO

Keywords:
Greenhouse gas emissions
Temporal variability
CO_2
Inversion
City

ABSTRACT

Constraining urban emissions is gaining more attention because of the important role of cities in reaching national climate mitigation targets. Urban inverse modelling studies could constrain emissions of large hotspots, but still face many challenges. It has been argued that more detailed information is needed on both atmospheric transport and prior emissions when moving to a higher spatial and temporal resolution. In this work we focus on the description of temporal variability in the prior emissions and examine how it impacts the optimization of urban emissions of CO_2, CH_4 and CO on a monthly time scale representative for a measurement campaign. Currently, temporal profiles based on long-term average activity data are often applied. However, these average temporal profiles are unable to capture a realistic variability in the emissions, such as those imposed by environmental conditions. Therefore, we created a set of location- and time-specific temporal profiles and compared the optimized emissions using these average and specific temporal profiles. We find that using the specific temporal profiles increases the optimized CO_2 emissions with 19%, even though the prior monthly emissions are the same. This suggests a change in the source-receptor relationship that affects comparison of the observed and simulated mixing ratios, leading to a different emission estimate. The impact is also large (~40%) for CH_4, but this is mainly due to the increase in prior emissions caused by redistributing agricultural emissions over all months of the year. Moreover, we show that extrapolating monthly emission estimates to annual estimates, required for reporting, using the various sets of temporal profiles can result in differences of max. 26% for CO_2, 101% for CH_4, and 13% for CO. Therefore, we conclude that an accurate representation of the temporal variability is essential for urban inverse modelling studies.

1. Introduction

The 2015 Paris Agreement describes a climate action plan to mitigate greenhouse gas (GHG) emissions globally (UNFCCC, 2015). The agreement specifies nationally determined emission reduction targets and obliges participating countries to monitor their progress towards achieving their targets. Currently, this reporting is performed annually based on national energy statistics (UNFCCC, 2020). Although this approach is reliable for carbon dioxide (CO_2), national emission estimates for methane (CH_4) and nitrous oxide (N_2O) are associated with relatively large uncertainties (Ganesan et al., 2015). Moreover, emission reporting is done with a lag of two years. Hence, there is a strong call for independent verification of the emissions (reductions) up to present year. For this purpose, inverse modelling frameworks have been developed to estimate emissions (trends) by combining monitoring network data and atmospheric transport models (Bergamaschi et al., 2018; Ciais et al., 2010). First experiences show that inversions can suggest improvements to national emission inventories, as illustrated by Ganesan et al. (2015) for the UK and Ireland.

Urban areas and associated industrial clusters are emission hotspots and responsible for about 70% of the global fossil fuel CO_2 emissions (IEA, 2008). Therefore, an important role is laid out for urban areas in reaching national (and global) climate mitigation targets as laid down in the Paris Agreement. Moreover, many large cities (e.g. C40 cities) have set their own ambitious climate goals. As urban areas often encompass a wide variety of human activities, they are very suitable to monitor the impact of measures in different source sectors and their combined effect. As such, exchange of best practices derived from verified emission

* Corresponding author.
E-mail address: ingrid.super@tno.nl (I. Super).

https://doi.org/10.1016/j.aeaoa.2021.100119
Received 4 March 2021; Received in revised form 30 June 2021; Accepted 3 July 2021
Available online 4 July 2021

reduction policies from frontrunner cities as encouraged by the Paris Agreement may benefit the policies implemented worldwide. Several scholars have examined the possibility to use inverse modelling to constrain urban fossil fuel GHG emissions (Breón et al., 2015; Hedelius et al., 2018; Kunik et al., 2019; Lauvaux et al., 2013, 2016; Nathan et al., 2018; Staufer et al., 2016; Ware et al., 2019). Although the results look promising, several challenges remain. For example, transport modelling and resolving sub-kilometre scale processes, combining different types of observations, and prior emissions information (Boon et al., 2016; Breón et al., 2015; Kort et al., 2013; Nathan et al., 2018). In this work we focus on the impact of the temporal variations in prior emissions on the inversions for urban areas. Improving the temporal variability has been recognized early as a key activity to improve GHG emission inversions (Peylin et al., 2011), although limited attention was given to the topic so far. Shortcomings in accounting for the temporal variability in the prior emissions may impact the quality of the inversions in several ways.

Firstly, the variability in emissions is, together with meteorological variability, the main driver for the variability in atmospheric concentrations of GHGs and air pollutants. Brophy et al. (2019) performed a simulation experiment in which the 'truth' is based on constant emissions and the prior uses temporally varying emissions. In their study, the temporally varying emissions were generated using average temporal profiles (hereafter: TPs), which are based on long-term average activity data (e.g. Breón et al., 2015; Denier van der Gon et al., 2011). With this approach Brophy et al. (2019) reached an uncertainty estimate of approximately 12% for three month-long measurement campaigns, which is comparable to the uncertainty estimate from atmospheric transport. Although these average TPs include typical seasonal and diurnal cycles, they do not include the impact of environmental and economic conditions. Studies within the air quality domain have shown that TPs that take into account environmental conditions improve the temporal correlation between observed and modelled timeseries and thus the link between emissions and concentrations (Hendriks et al., 2015; Mues et al., 2013). Moreover, Guevara et al. (2021) have shown significant reductions in emissions from road transport and industrial activities during COVID-19 lockdown periods, but also changes in day-to-day variability. Understanding the impact of these lockdowns, which induce deviations from statistical average activities and associated TPs, on local emissions is valuable information for policy-makers and scientists worldwide, but is impossible to assess without COVID-specific TPs.

Secondly, an incorrect representation of the temporal variability in emissions can negatively impact the total emission estimate derived from short-term measurement campaigns and inversions using a time-of-the-day selection criterion (Super et al., 2020b). Although extensive observational networks are currently available around a number of megacities (Breón et al., 2015; Hedelius et al., 2018; Turnbull et al., 2015), such infrastructure is still relative scarce. This makes targeted measurement campaigns, that typically cover shorter periods, indispensable to verify GHG emissions in the future. To arrive at annual emissions, needed for reporting, an extrapolation is required using a description of the temporal variability within a year. A similar approach is needed when a subset of a time series is used in an inversion. For example, some inversions use only daytime observations to favour well-mixed conditions (Boon et al., 2016; Breón et al., 2015; Lauvaux et al., 2013). Deriving near real-time information on the impact of (temporary) mitigation measures, such as the COVID-19 lockdowns, will encounter the same challenge.

Thirdly, using different TPs may affect the outcome of an inversion through the prior uncertainty. Whereas the uncertainty in country-level emissions is often well-defined, the uncertainty in high-resolution emission maps is not well-known. Spatiotemporal downscaling results in additional uncertainties that need to be taken into account. Although efforts have been made to better quantify the prior emission uncertainties (Andres et al., 2016; Gately and Hutyra, 2017; Hutchins et al., 2017; Super et al., 2020b), the impact of improved uncertainties on inverse modelling results has not yet been examined in detail.

Hence, we argue that an accurate description of the prior emission timing can alleviate several problems currently faced in urban inversion studies. The goal of this paper is to quantify the impact of the TPs and the prior emission uncertainty on the inverted emissions of the GHGs CO_2 and CH_4 and co-emitted species CO for the Rotterdam-Rijnmond region in the Netherlands. With the results we aim to show the potential of short-term campaigns to evaluate emission strengths from cities or specific sources. The research questions are:

1. How well can we describe the temporal variability in human activities that cause emissions of CO_2, CH_4 and CO and how does this affect the prior uncertainty? (Sect. 3.1)
2. How do the TPs affect simulated mixing ratios of CO_2, CO and CH_4? (Sect. 3.2)
3. What is the impact of the TPs and prior uncertainties on monthly emission estimates? (Sect. 3.3)
4. What is the impact of the TPs on the extrapolation of monthly to annual emissions? (Sect. 3.4)

2. Materials and methods

We selected the Rotterdam-Rijnmond (RR) region in the Netherlands to investigate the impact of the specification of the temporal variability and uncertainty of the prior emissions for short-term monitoring with a limited number of stations. This region was selected for its variety of source sectors and the availability of three stations with high quality observations around the main source area. After a short description of the case study region we detail the a-priori emission preparation and inversion framework used.

2.1. Case study

For the case study we nest the RR-domain region in a larger domain covering the Netherlands entirely and some major source areas in Germany (Ruhr area) and Belgium (Antwerp) (NL-domain). Fig. 1 shows the domains and the emissions for the RR-domain. At the centre of the RR-domain lies the city of Rotterdam with ~625,000 inhabitants. To the west of the city the largest sea port of Europe is located, dominated by industrial activities clearly visible on the map with point source emissions.

The inversions cover a period of one month (January 2015), illustrative for a short-term measurement campaign, to illustrate the importance of a correct representation of the temporal variability when applying extrapolation to a full year. We hypothesize that one month is short enough to still have some effect of random errors in the emission timing, but long enough to be meaningful for an annual emission estimate. Besides the greenhouse gases CO_2 and CH_4 we also include CO in our simulations, because CO is co-emitted with CO_2 from fossil fuel burning activities and can provide information on which of the source sectors causes the largest discrepancies.

In this study we used the observations of CO_2, CH_4 and CO from three sites within the RR-domain (see Fig. 1). The first site, Westmaas, is located 15 km south of the city centre of Rotterdam. The second site, Zweth, is 7 km northwest of Rotterdam. Both sites are equipped with cavity ring-down spectroscopy analysers (Picarro Inc., type G2401) sampling air from an inlet of 10 m a.g.l. For a detailed description of these two sites we refer to Super et al. (2017b). The Zweth measurement site is close to the Rotterdam-The Hague airport from which standard meteorological observations were obtained. A third site, Cabauw, is located 32 km east of the centre of Rotterdam (Van der Laan et al., 2016; Vermeulen et al., 2011). Cabauw is the experimental supersite for atmospheric composition in the Netherlands, for which long-term observations of CO_2 and CH_4 are available from several heights along a tall tower. For CO_2 and CH_4 we used the observations at 60 m a.g.l., whereas CO is measured at ground level only (Frumau et al., 2020). Given the

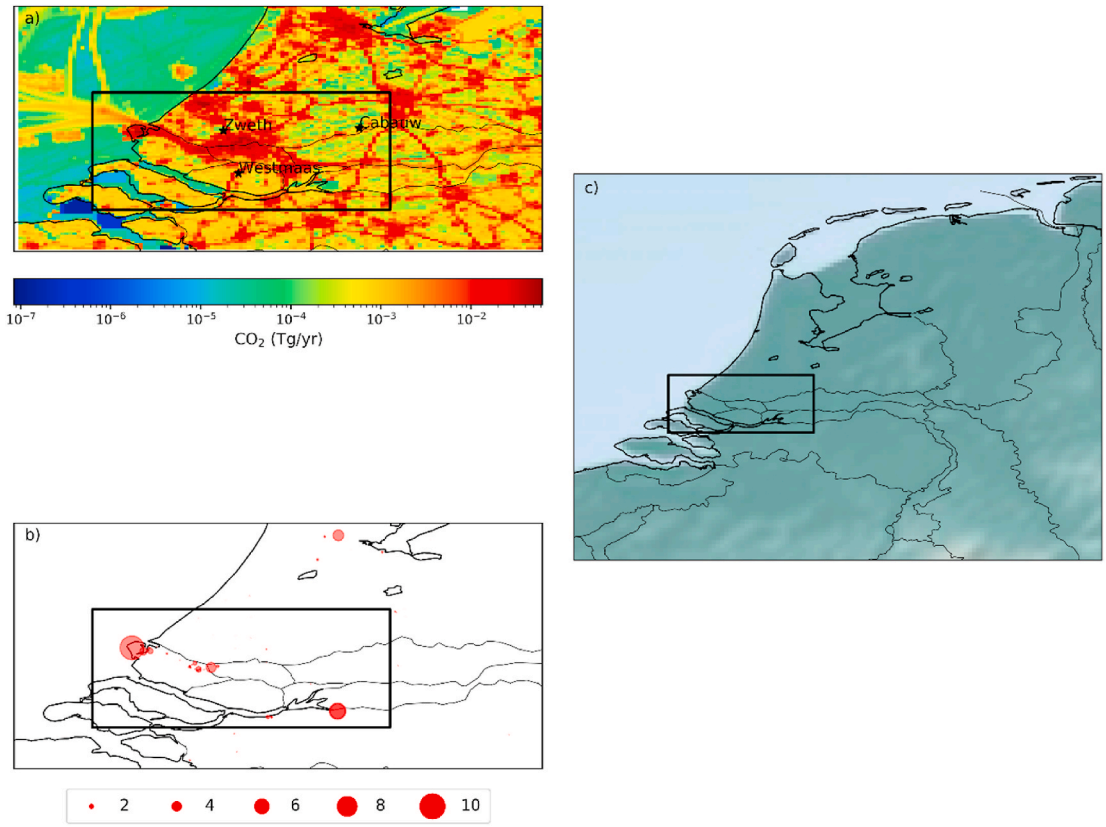

Fig. 1. Emissions maps of CO_2 (Tg yr^{-1}) for the RR-domain, both for a) area sources and b) point sources. C) Model domains with a horizontal resolution of 1/10° longitude x 1/20° latitude (NL-domain) and 1/60° longitude x 1/120° latitude (RR-domain). The RR-domain is represented by a black box. Black stars represent the measurement locations.

dominant wind direction from the southwest Zweth and Cabauw are often strongly affected by urban/industrial emissions, although the plumes are more strongly diluted by the time they arrive in Cabauw. The area between Rotterdam and Cabauw is dominated by agricultural activities and Cabauw is a good site to constrain agricultural emissions.

2.2. Emission data

The prior emission dataset for 2015 is developed by TNO and described by Super et al. (2020b). The emission map covers western Europe (Netherlands, Germany, Belgium, parts of France and the UK, and several other countries) at a resolution of 1/60° longitude x 1/120° latitude (~1 × 1 km^2). It is based on the reported emissions by European countries to the UNFCCC (greenhouse gases) and to EMEP/CEIP (European Monitoring and Evaluation Programme/Centre on Emission Inventories and Projections, air pollutants). These emissions have a high level of detail, but are aggregated to 12 GNFR sectors after spatial downscaling using proxy maps. For road transport emissions are provided per fuel type. For large point sources the exact location and reported emission is used when available (e.g. from the E-PRTR (European Pollutant Release and Transfer Register)). Table 1 summarizes the sectoral emissions for each trace gas. Fig. 1 shows the emissions for the RR-domain from both the area and point sources.

The a-priori total emissions for the RR-domain in 2015 were estimated to be 59.7 Tg CO_2, 91.5 Gg CO and 75.8 Gg CH_4. The CO_2 emissions come from a variety of human activities, such as road transport and industry clustered in urban regions. During combustion CO is co-emitted with CO_2 in an emission ratio that is determined by the combustion characteristics (completeness of combustion, type of fuel, etc.). In contrast, CH_4 emissions show a very different pattern as these emissions are often not related to fossil fuel combustion. Two important source sectors are fugitives and waste, which are often larger in more densely populated areas. For example, waste treatment takes place close to where the waste is produced, i.e. near urban/industrial areas. However, another important source of CH_4 is agriculture (livestock). In our case study region there is a lot of agricultural activity taking place in close proximity to the urban centres.

Table 1
Emissions for 2015 per sector in Tg yr^{-1} (CO_2) or Gg yr^{-1} (CH_4 and CO) and between brackets the sectoral contribution (in %) to the total emission per species. Contributions <1% are not given.

Sector	NL_domain			RR_domain		
	CO_2	CH_4	CO	CO_2	CH_4	CO
A_PublicPower	203 (41)	23 (2)	50 (3)	31 (52)	1 (1)	2 (2)
B_Industry	136 (27)	112 (9)	719 (47)	14 (24)	5 (6)	10 (11)
C_OtherStationaryComb	73 (15)	72 (6)	199 (13)	5 (9)	6 (9)	9 (10)
D_Fugitives	5 (1)	70 (5)	–	–	11 (15)	–
E_Solvents	–	–	–	–	–	–
F_RoadTransport_exhaust	65 (13)	–	418 (27)	5 (9)	–	53 (58)
G_Shipping	11 (2)	–	18 (1)	3 (5)	–	4 (5)
H_Aviation	–	–	8 (1)	–	–	–
I_OffRoad	3 (1)	–	116 (8)	–	–	13 (15)
J_Waste	–	226 (18)	–	–	24 (32)	–
K_AgriLivestock	–	765 (60)	–	–	27 (36)	–
L_AgriOther	–	–	–	–	–	–

2.2.1. Average temporal profiles

A set of default TPs per GNFR sector was used as the 'average' set (Fig. 2), based on TPs originally developed for air quality modelling applications by Denier van der Gon et al. (2011). These TPs were calculated using a scaling factor for the month of the year, the day of the week and the hour of the day. These factors describe e.g. the patterns in seasonal heating demand, in the reduced economic activity during the weekend, and in traffic intensity during the day. Using these average TPs, the a-priori emissions for January 2015 are 5.89 Tg CO_2, 7.715 Gg CO and 5.08 Gg CH_4 for the RR-domain.

2.2.2. Location- and time-specific temporal profiles

A set of location- and time-specific TPs (hereafter: specific TPs) was developed using local activity data. We only created specific TPs for the public power, other stationary combustion, road transport, and agriculture-livestock sectors. The reasons for this selection are that these sectors have a lot of variability, are important sources of the selected pollutants (Table 1), and the relevant data were available to improve the average TPs.

For public power (GNFR_A) detailed activity data are available from the European Network of Transmission System Operators for Electricity (ENTSO-E). The data are available per country and fuel type and we use average data for the Netherlands for gas, coal and biomass. For the simulation with specific TPs we applied the fuel-specific TPs to the point sources in OPS, whereas the residual power plant emissions (i.e. small sources not reported to point source databases) got the TP for gas.

The other stationary combustion sector (GNFR_C) mostly consists of heating (commercial and residential). The degree day method (Mues et al., 2014) using the outside temperature measured at Rotterdam-The Hague airport was used to calculate the specific TP. This methodology describes the temporal variations in emissions as a function of the outside temperature, taking into account a fixed amount of energy consumption used for cooking and warm water supply. We used the heating degree day method to get daily emission intensities and adopted the diurnal cycles from smart meter data (i.e. separate TPs for weekdays and weekends) (Liander, 2020).

For road transport (GNFR_F) traffic counts were collected for different road types (highway, main roads and urban roads) in and around Rotterdam. All selected locations distinguish at least 3 vehicle types (if more, they were aggregated): cars, light-duty vehicles (LDV) and heavy-duty vehicles (HDV). Given the gaps in the traffic count time series and the fact that large spatial variations exist in traffic patterns, we created average monthly, weekly and daily TPs for the entire region for each road and vehicle type. The daily cycles were made separately for weekdays and weekends/holidays. To get one TP per fuel type we weighted the contribution of the different vehicle and road types.

Finally, we updated the TPs of the agricultural sector. The agricultural sector consists of two sub-sectors: agriculture-livestock and agriculture-other. The CH_4 emissions from agriculture-livestock are dominated by enteric fermentation, which is an important source of CH_4. The agriculture-other sector is dominated by manure/fertilizer application, which is mainly important for ammonia. As shown in Fig. 3 the average TPs are very different for both sub-sectors, with no emissions from agriculture-other in January. Unfortunately, in a previous version of the emission dataset the emissions from enteric fermentation were accidently assigned to the agriculture-other sector, meaning that an important source of CH_4 was missing in January. So we represented the temporal variations in agriculture-livestock using the agriculture-other TP in the average set and the agriculture-livestock TP in the specific set. Although this error is much larger than what inverse modellers are normally looking for, we included this experiment to illustrate the impact of missing sources.

The resulting TPs and the comparison to the average TPs are discussed in Sect. 3.1.

2.2.3. Emission uncertainties

The high-resolution emission dataset described in Sect. 2.2 is prepared using a wide range of data. Emissions are calculated as the product of activity data (e.g. fuel consumption) and emission factors. The spatial disaggregation was done using proxy maps and the temporal disaggregation makes use of TPs based on activity data. All these data have a certain level of uncertainty, which can be used to calculate the total emission uncertainty for the RR-domain and case study period. We use a Monte Carlo method for this, as described in detail by Super et al. (2020b). The final uncertainties from the Monte Carlo analyses using average and specific TPs are shown in Table 2. These values populate the diagonal of the prior error covariance matrix P (see Sect. 2.3 for further explanation). The off-diagonal values are set to zero, meaning that the errors are not correlated. Note that the overall uncertainties change when using specific TPs due to a shift in the importance of each source sector, with more uncertain sectors becoming more dominant.

To study the impact of prior uncertainties on the optimization of emissions we also applied a second uncertainty estimate motivated by other scientific studies. The Monte Carlo-based uncertainty for CO_2 was estimated to be only ~5%, which is lower than generally used in urban inversions. Bréon et al. (2015) assume a 20% uncertainty in their monthly CO_2 inventory for Paris. Similarly, Graven et al. (2018)

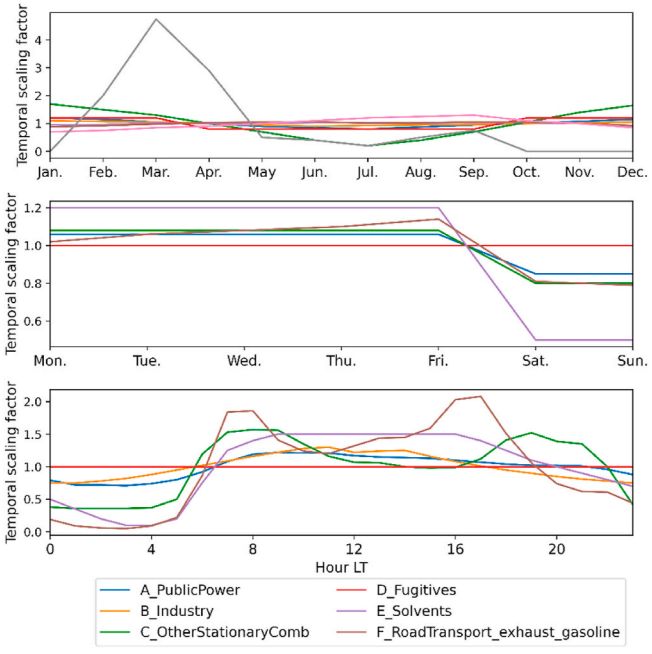

Fig. 2. Temporal scaling factors for the month of the year, day of the week and hour of the day per GNFR sector. This set is denoted as the 'average' set of TPs. TPs are not shown for those source sectors that have no variability. The TPs for road transport – exhaust – gasoline are also valid for diesel and LPG.

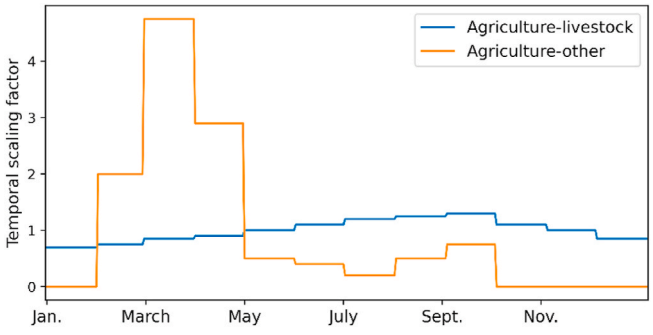

Fig. 3. Average TPs (daily data) for the agriculture-other and agriculture-livestock sectors.

Table 2
Prior uncertainty estimates for the case study domain and 1-month period based on the Monte Carlo approach using average and specific TPs and based on a literature review.

	Average TPs	Specific TPs	Literature-based
CO_2	4.7%	4.6%	20%
CO	21.2%	24.9%	80%
CH_4	40.7%	49.2%	200%

estimated the uncertainty in the CO_2 emissions for California to be 18–19%. Lauvaux et al. (2016) found an aggregated error variance of 25% for Indianapolis for a 5-day period. These values are about 4–5 times higher than we estimated here. For CH_4 uncertainty estimates are even more sparse and variable. For example, Ganesan et al. (2015) used a lognormal standard deviation of 50% for national scale CH_4 emissions for the UK/Ireland. In contrast, with the Monte Carlo approach we estimate the total annual emission uncertainty for CH_4 in the whole of the Netherlands to be about 10%, which is similar to the official reported uncertainty of 9% for the Netherlands. From this literature overview we conclude that the uncertainties vary a lot between different studies, also depending on the spatial and temporal resolutions. Nevertheless, values used in literature are generally higher than what we calculated with the Monte Carlo approach. Therefore, we used a second set of uncertainties that are about 4–5 times higher than the Monte Carlo-based uncertainties (Table 2).

2.3. Inverse modelling framework

The basis of our inverse modelling framework is the CarbonTracker Data Assimilation System (CTDAS) (v1.0) described in more detail by Van Der Laan-Luijkx et al. (2017) and used previously for urban applications (Super et al., 2020a). CTDAS uses an Ensemble Kalman Filter approach (Whitaker and Hamill, 2002), which optimizes the cost function for all variables in the state vector x using information from observations (y^0 with covariance R) and starting from a prior estimate of the state vector (x^b with covariance P):

$$J(x) = \left(y^0 - \mathscr{H}(x)\right)^T R^{-1} \left(y^0 - \mathscr{H}(x)\right) + \left(x - x^b\right)^T P^{-1} \left(x - x^b\right) \quad (1)$$

Here, $\mathscr{H}$ is the atmospheric transport model (observation operator) that returns simulated mole fractions given the state vector. R and P determine how much weight is given to the observations and prior estimate, respectively. See sections 2.2.3 and 2.3.3 on how the R and P matrices are defined.

The optimized state vector (indicated with superscript a, whereas b refers to the prior estimates) which minimizes the cost function is

$$x^a = x_t{}^b + K\left(y_t{}^0 - \mathscr{H}\left(x_t{}^b\right)\right) \quad (2)$$

and its covariance is

$$P_t{}^a = (I - KH)P_t{}^b \quad (3)$$

Here, H is the linearized observation operator and K is the Kalman gain matrix:

$$K = \left(P_t{}^b H^T\right)\left(HP_t{}^b H^T + R\right)^{-1} \quad (4)$$

We calculated the solutions of Eq. (2) and Eq. (3) using an ensemble of 20 members. The dimensions of our inverse problem are N = 1726, 1283 and 1801 observations of CO_2, CH_4 and CO, respectively, and M = 3 unknowns. We replaced the global TM5 transport model originally integrated in CTDAS with a combination of the regional LOTOS-EUROS model and the OPS plume model. More details about the individual parts of the inversion system are provided in the following sections.

2.3.1. Observation operator

The observation operator consists of two models: LOTOS-EUROS (v2.2) for the NL-domain and area sources in the RR-domain (see Fig. 1 for domains); OPS (v10.3.5) for the point sources in the RR-domain. We use the OPS model for point sources that are relatively close to the measurement sites, because a grid-based model like LOTOS-EUROS tends to overestimate the dilution of such sources (Boon et al., 2016; Vogel et al., 2013). The grid resolutions of LOTOS-EUROS are 1/10° longitude x 1/20° latitude (NL-domain) and 1/60° longitude x 1/120° latitude (RR-domain).

LOTOS-EUROS is an open-source, regional chemical transport model with both scientific and operational applications (Manders et al., 2017). It was mainly developed for air quality modelling, but is also applied for greenhouse gases. The model includes labelling options for source apportionment and has been used for data assimilation (Curier et al., 2012; Kranenburg et al., 2013). LOTOS-EUROS is an offline model that uses meteorological data obtained from other models. Here, we use meteorological data produced by the COSMO model (Baldauf et al., 2011) with a resolution of 0.05 × 0.05° and 40 vertical layers up to 10 km, which is interpolated to the LOTOS-EUROS grid. The boundary conditions of CO_2, CO and CH_4 mixing ratios for the largest NL-domain are taken from a high-resolution (0.14 × 0.14°) IFS run (https://www.ecmwf.int/en/research/modelling-and-prediction) with full chemistry (C-IFS). The mixing ratios calculated by LOTOS-EUROS for the NL-domain are used as boundary conditions for the RR-domain. Biogenic fluxes are calculated with the Vegetation, Photolysis, and Respiration Model (VPRM) (Mahadevan et al., 2008) at a 5 × 5 km^2 resolution. The anthropogenic emissions were labelled to be able to separate between fossil fuel emissions from the RR-domain and all other processes (large-scale background, biogenic fluxes, fossil fuel emissions from outside the RR-domain). Note that average TPs are used for the NL-domain (except for agriculture), so that the boundary conditions for the RR-domain are exactly the same for all experiments.

OPS (short-term version) is a plume dispersion model that provides hourly atmospheric concentrations at receptor locations (Van Jaarsveld, 2004; Sauter et al., 2016). It works with forward trajectories, taking into account time-varying transport, and applies a Gaussian plume formulation to calculate the concentrations. The OPS model is driven by spatially interpolated meteorological observations from the Royal Dutch Meteorological Institute.

The influence time for the urban observations is set at 10 h, i.e. emissions from more than 10 h ago do no longer affect the current observations, which is based on the size of the RR-domain and typical wind speed. Therefore, we run the OPS model from −10 h to the time of observation to calculate concentrations. For LOTOS-EUROS we only perform one monthly simulation per set of TPs and apply the ensemble of scaling factors directly to the calculated concentrations (only that part labelled as coming from local emissions), assuming a linear relationship between emissions and concentrations. Although this method neglects the influence of atmospheric chemistry, we believe that this simplification has little impact on our findings due to the relatively short influence time compared to the relatively long chemical lifetime of the trace gases included in this work.

2.3.2. State vector and propagation

The state vector consists of one scaling factor for the entire RR-domain per trace gas, i.e. a total of 3 scaling factors with a prior value of 1.0. We optimize the state vector for each day individually, starting each new day with the optimized scaling vector. In other words, the information gained from the previous day is propagated. The prior emission uncertainties (Sect. 2.3.4) are reset each day to give the state vector freedom to move away from its prior. Having daily scaling factors helps to identify the source sectors that are likely causing the largest errors, especially in combination with the wind direction, multiple trace gases and the difference between the two sets of TPs. Although such a detailed study is beyond the scope of this work, we use propagation to demonstrate the applicability of this approach.

2.3.3. Selection of observations

To favour well-mixed conditions, which have a lower model error, inverse modelling studies often select daytime observations. Here, we choose a different selection criterion, namely observations when the wind speed is at least 3 m s^{-1}. The advantage of this method is that all hours of the day are sampled (Fig. 4), so that a structural error in the diurnal emission timing will have less impact on the results. On the downside, we may introduce uncertainty by modelling night time conditions. Nevertheless, it was argued that a selection based on meteorological conditions could actually be more suitable than a selection based on the time of the day (Martin et al., 2019). We have compared the inversion results using the wind speed and hour of the day selection criteria and found that the posterior residuals were smaller using the wind speed criterion (not shown).

Besides the uncertainty in the prior emissions we also need to consider the uncertainties caused by the model transport, interpolation and observations. These uncertainties are based on typical errors in the comparison of the simulated and observed mixing ratios and are set at 2.5 ppm (CO_2), 15 ppb (CH_4) and 8 ppb (CO), which populate the diagonal of the R matrix. We assume these uncertainties are not correlated (i.e. off-diagonal R values are set to zero).

2.4. Experiments

We performed three experiments, which are listed in Table 3. The 'Base' and 'Uncertainty' runs use the average TPs, whereas the 'Specific' run uses the specific TPs. Both the 'Base' and 'Specific' runs start with a prior uncertainty based on the Monte Carlo approach. The 'Uncertainty' run uses the uncertainty estimate from literature. Otherwise the runs are exact copies.

The results from the inversions are used to answer research questions 3 and 4. The monthly scaling factors are calculated as the mean of the daily scaling factors. To examine the impact of uncertain TPs on the extrapolation of monthly to annual emissions we compare the annual emissions using extrapolation with the average and specific TPs. The prior and optimized monthly emissions ($E_{prior,\ month}$ and $E_{opt,\ month}$) for the 'Base' and 'Specific' experiment are calculated as follows:

$$E_{prior,month} = E_{prior,year} / 12 \cdot t_{month,average} \quad (5)$$

$$E_{opt,month} = E_{prior,month} \cdot optimized\ scaling\ factor \quad (6)$$

Here, $E_{prior,\ year}$ is the prior annual emission and $t_{month,\ average}$ is the monthly temporal scaling factor from the average set of TPs. The optimized annual emissions using the average TPs are

$$E_{opt,average,year} = E_{prior,year} \cdot optimized\ scaling\ factor \quad (7)$$

Using the specific TPs the optimized annual emissions are

Table 3
Overview of experiments and their settings.

Name	TPs	Prior uncertainty
Base	Average	Monte Carlo
Uncertainty	Average	Literature
Specific	Specific	Monte Carlo

$$E_{opt,specific,year} = E_{opt,month} / t_{month,specific} \cdot 12 \quad (8)$$

where $t_{month,\ specific}$ is the monthly temporal scaling factor from the specific set of TPs. The optimized annual emissions using the different sets of TPs are related as follows:

$$E_{opt,specific,year} \ / \ E_{opt,average,year} = t_{month,average} / t_{month,specific} \quad (9)$$

For the 'Specific' experiment the subscript 'average' and 'specific' in the above equations are switched.

3. Results

3.1. Location- and time-specific temporal profiles

The specific and average TPs for public power (GNFR_A) are shown in Fig. 5. The average TPs have been developed mainly for air pollutants, which are primarily emitted by coal-fired power plants which were thought to show little short-term variability. Therefore, the average TP mostly represents the seasonal variability in the coal-fired power plant emissions. However, gas-fired power plants show more short-term variability, and also coal-fired power plants show increasingly more short-term variations. These are not captured well and the agreement between the average and specific (data-based) TPs is limited ($R^2 = 0.34$

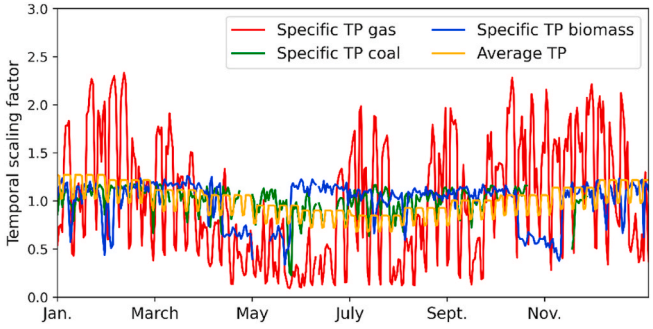

Fig. 5. Specific TPs (daily data) for power plants based on ENTSO-E data, separately for gas, coal and biomass. The average TP is also shown.

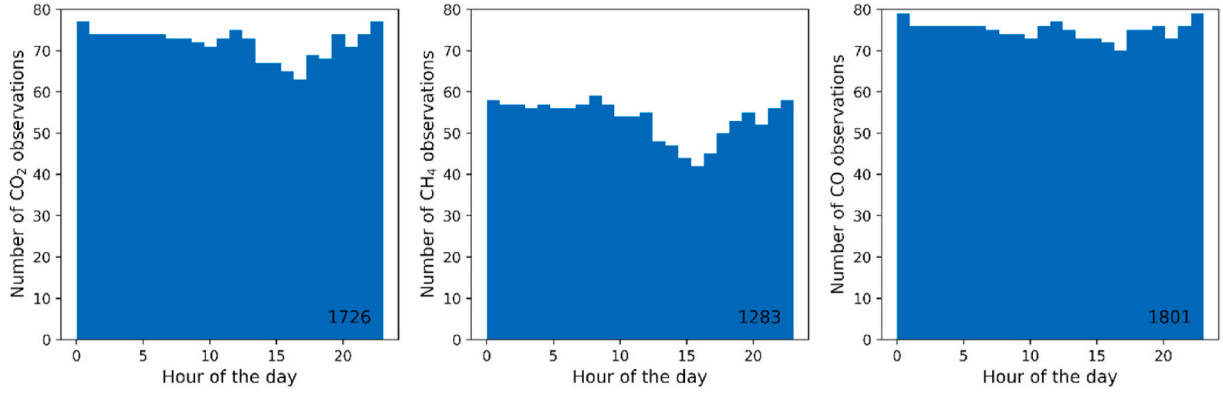

Fig. 4. Total number of observations for each hour of the day after selecting for wind speed. The observations of CH_4 which are used for the bias correction are also excluded here. The total number of observations for the whole period is given.

(gas), 0.19 (coal) and 0.004 (biomass) for 2015; $R^2 = 0.45$ (gas), 0.27 (coal) and 0.01 (biomass) for January 2015). Apparently, the day-to-day variations in emissions from coal-fired power plants are captured less well than those in the emissions from gas-fired power plants.

We compare the average and specific TPs from other stationary combustion (GNFR_C) to the activity reported by smart meters (Liander, 2020) (Fig. 6) and find a much better agreement with the specific TP ($R^2 = 0.90$ for 2015; $R^2 = 0.81$ for January 2015) than with the average TP ($R^2 = 0.65$ for 2015; $R^2 = 0.02$ for January 2015). Moreover, the smart meter data provides information on the diurnal variations. The average TP represents the average diurnal cycle for weekdays very well ($R^2 = 0.84$), but less for weekends and holidays ($R^2 = 0.68$). We use the heating degree day method to get daily emission intensities and adopt the diurnal cycles from the smart meter data (i.e. separate TPs for weekdays and weekends).

The average TPs for road transport (GNFR_F) (Fig. 7) are mainly based on cars, which are dominated by gasoline exhaust, and there is a better agreement with the specific TP for gasoline ($R^2 = 0.84$ for 2015 and January 2015) than for diesel ($R^2 = 0.70$ for 2015 and January 2015). Diesel is more dominated by HDV, which shows a different weekly and diurnal cycle. LPG is much less used, but is represented relatively well by the average TP ($R^2 = 0.85$ for 2015; $R^2 = 0.86$ for January 2015).

With the specific TPs, we estimate the prior emissions for January 2015 to be 5.90 Tg CO_2, 8.50 Gg CO and 6.29 Gg CH_4 for the RR-domain (compared to 5.89 Tg CO_2, 7.715 Gg CO and 5.08 Gg CH_4 using the average TPs). The uncertainties from the Monte Carlo analyses using the specific TPs are 4.6% for CO_2, 24.9% for CO, and 49.2% for CH_4 (Table 2). The overall uncertainties are slightly higher for CO and CH_4 when using specific TPs. In this case, the CH_4 agriculture-livestock emissions are missing when using average TPs and therefore they do not affect the uncertainty. However, this is a very large sector and when adding them using the improved TP there are more emissions with a relatively large uncertainty added. Similarly, for CO there is an increase in household emissions, which also have an above-average uncertainty.

3.2. Validation of forward simulations

A first check of the forward model simulations reveals a significant bias in the CH_4 ratios, also when sampling relatively clean background air (Fig. 8). This suggests there is a bias in the large-scale background, which could cause an incorrect attribution of the model-data mismatch to local emissions. Although the background or boundary conditions can be optimized, this option is currently not part of our framework. Instead, we decided to apply a bias correction on the prior CH_4 mixing ratios using background data.

We assume a mixing ratio of less than 2000 ppb to be relatively free of local emission contributions and select all data points with a simulated and observed mixing ratio of less than 2000 ppb to calculate the bias in the background (simulated – observed). We only use observations from Westmaas and Cabauw for this bias correction, as these locations are more likely to sample air representing background concentrations. Both sites show a similar mean bias of 30.5 (Westmaas) and 33.3 ppb (Cabauw) with specific TPs and 32.3 (Westmaas) and 42.3 (Cabauw) with average TPs, resulting in a bias correction of 31.9 (specific) and 37.3 ppb (average). The data used for the bias correction are not assimilated to avoid contamination, but since these background data do not contain much information on local emissions they are of little use to the inversion.

A comparison of daily mean mixing ratios (after bias correcting CH_4) is shown in Fig. 9. The difference between the model simulations using the average and specific TPs is limited, because the large-scale background dominates the CO_2 and CH_4 mixing ratios. The correlation with the observations is similar for both runs, with a good agreement for all species. However, the run with specific TPs is often closer to the 1:1 line, especially for CO_2 and CO at the locations that are often affected by local enhancements (Zweth, and to a lesser extend also Westmaas). This suggests that days with high local enhancements are better represented with specific TPs, whereas they are often underestimated when average TPs are used.

3.3. Monthly emission calculations

Comparing the optimized monthly emissions from the three experiments reveals that the TPs can affect the optimization in several ways (Fig. 10). First, the prior monthly emissions can be different. Second, the comparison of hourly observed and simulated mixing ratios is affected, even if the monthly emissions remain similar. Third, the prior uncertainty can be different when relatively uncertain source sectors get more or less weight. We also clearly see that the impact of different TPs is larger than the impact of an increased prior uncertainty. However, there is an interplay between the prior uncertainties and the difference between the two sets of TPs. All of these aspects will be discussed in more detail.

In the case of CH_4 the main difference is the inclusion of emissions from agriculture-livestock in the 'Specific' experiment. This is an important sector, but also highly uncertain. Fig. 10 shows that the CH_4 emissions have a large prior uncertainty and the optimized emissions using specific TPs are much higher than for the 'Base' experiment. The most likely explanation is that agricultural emissions are strongly underestimated and that the contributions of other sectors do not correlate with those of agriculture. Therefore, in the absence of agricultural emissions in the 'Base' experiment, scaling is entirely ineffective. This results in lower optimized emissions for the 'Base' experiment. The improved representation of the agricultural emissions in the 'Specific' experiment provides the inversion system the degrees of freedom to pull close to the observations.

In contrast, for CO_2 and CO the prior monthly emissions are nearly

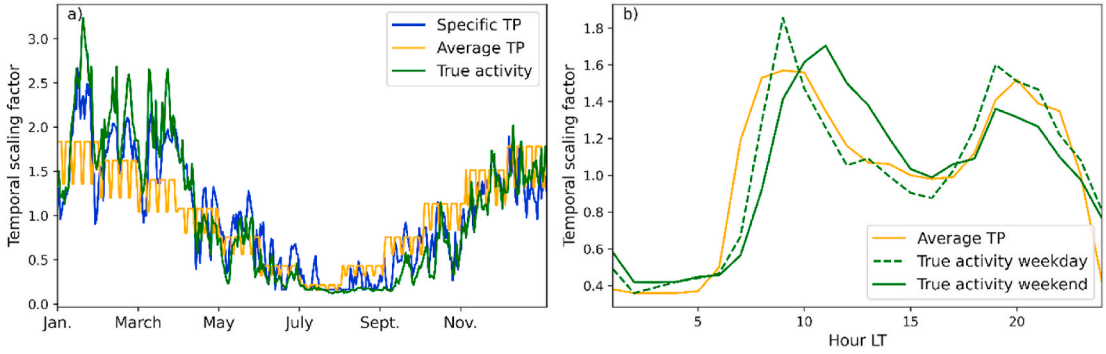

Fig. 6. a) Specific TP (daily data) for small combustion based on degree days, compared to true activity (smart meter data) and the average TP. b) Diurnal cycle in true activity (smart meter data) for weekdays and weekends/holidays (hour LT), compared to the average TP.

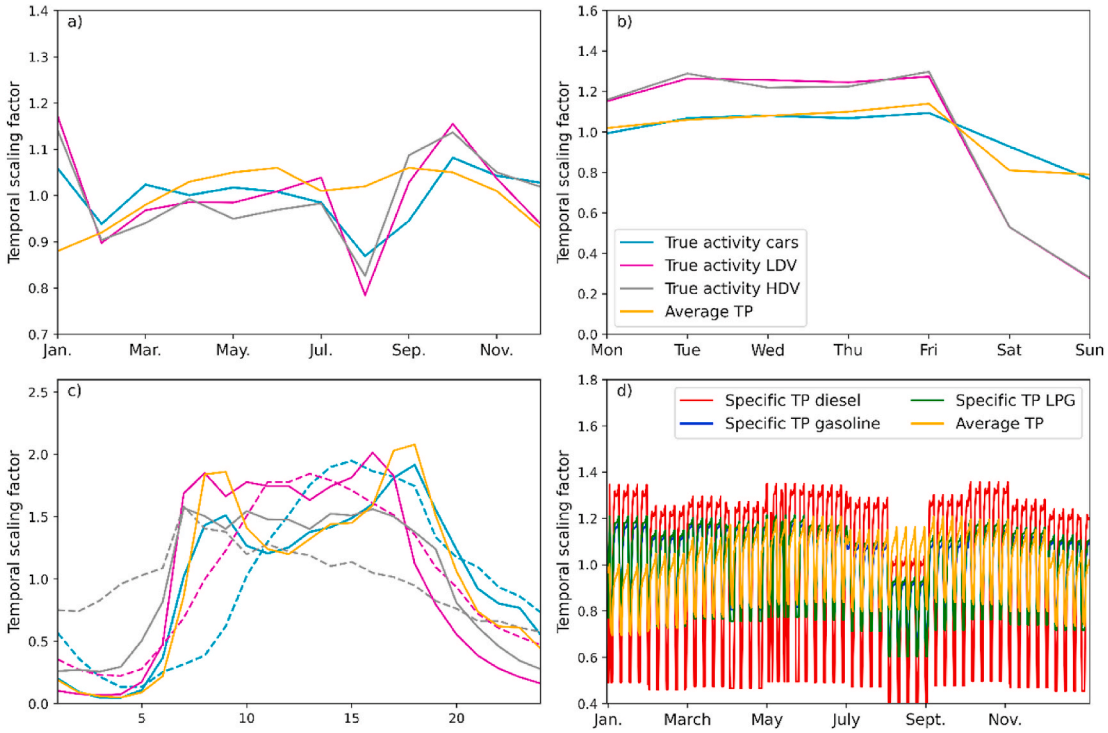

Fig. 7. a) Monthly variations, b) weekly variations, and c) daily variations (weekdays (full lines) and weekends (dashed lines)) in traffic counts per vehicle type, only for main roads; d) Specific TPs per fuel type for all roads combined. The average TPs are also given.

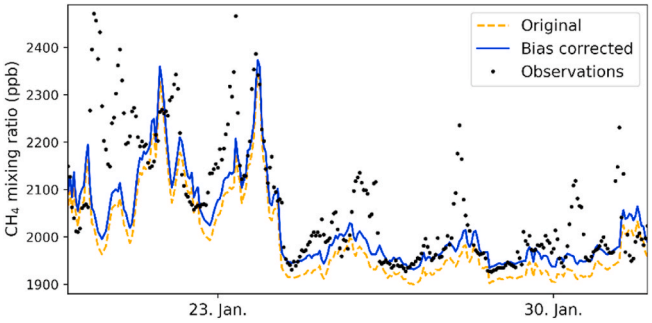

Fig. 8. Zoom on time series of CH_4 mixing ratios at Westmaas simulated by LOTOS-EUROS + OPS (yellow dashed line) and observed (black dots). After the bias correction the simulated mixing ratios are closer to the observations (blue line). (For interpretation of the references to colour in this figure legend, the reader is referred to the Web version of this article.)

similar using the two sets of TPs. However, the prior uncertainty in CO_2 emissions is small, whereas the prior uncertainty in CO emissions is relatively high. Nevertheless, they are similar for the 'Base' and 'Specific' experiments and therefore the main difference between these experiments is the hourly variability. We find that the optimized CO_2 emissions are much higher for the 'Specific' experiment, despite the small difference in simulated time series (Fig. 9), whereas it is similar to the 'Base' experiment in the case of CO. This suggests that the difference between simulated and observed mixing ratios at hourly resolution has a significant effect on the optimization of monthly emissions, especially when the prior uncertainty is small. With a relatively high prior uncertainty less information is taken from the prior and more weight is given to the observations (Eqs. (2) and (4)) and hence the impact of a different prior is limited. Thus the optimized emissions of CO are mostly the result of a fit to the observations.

This is also reflected in Fig. 11, which shows the daily variations in scaling factors for the different experiments. The CO scaling factors are similar for all experiments, so the impact of the prior data and uncertainty is limited. In contrast, the CO_2 scaling factors show large day-to-day differences between experiments, even though the final CO_2 scaling factor is similar for the 'Base' and 'Uncertainty' experiments. The difference between the 'Base' and 'Specific' experiments suggests a change in the source-receptor relationship that affects the outcome of the inversion, despite starting with the same overall emissions. Updating the time profiles affects the dominance of each source sector at any given moment, changing the entire emission landscape. This is especially true for sectors that are influenced by synoptic meteorological conditions, such as residential heating. Generally, colder conditions in our study domain occur with an easterly wind, increasing the emissions from other stationary combustion compared to a period with a westerly wind. This causes a systematic bias in the source-receptor relationship when these differences are not taken into account. Indeed, the first 2 weeks of 2015 and the period from 25 to 28 January were a lot warmer than average with a westerly wind, resulting in a stronger decrease in the 'Base' scaling factors to compensate for this.

3.4. Annual emission calculations

Based on the results of our campaign-like inversion we can estimate annual emissions using extrapolation with the various sets of TPs. Fig. 12 shows the optimized annual emissions following from Eq. (7) and Eq. (8). The difference between the 'Average TP' and 'Specific TP' case reflects the difference in the monthly temporal scaling factors (Eq. (9)). So the larger the error in the TP for the period in which a measurement campaign is done, the larger the error in the annual estimate. The prior yearly emissions from the TNO emission inventory are indicated by the dashed line.

We find small differences between the 'Average TP' and 'Specific TP' cases for CO_2. Indeed, the temporal scaling factors in January are very similar (Fig. 13). The annual CO_2 emissions are relatively well-known, with an estimated uncertainty of ~2%. Whereas the 'Base' experiment deviates significantly more from the annual prior than its estimated uncertainty, both annual emission estimates for the 'Specific'

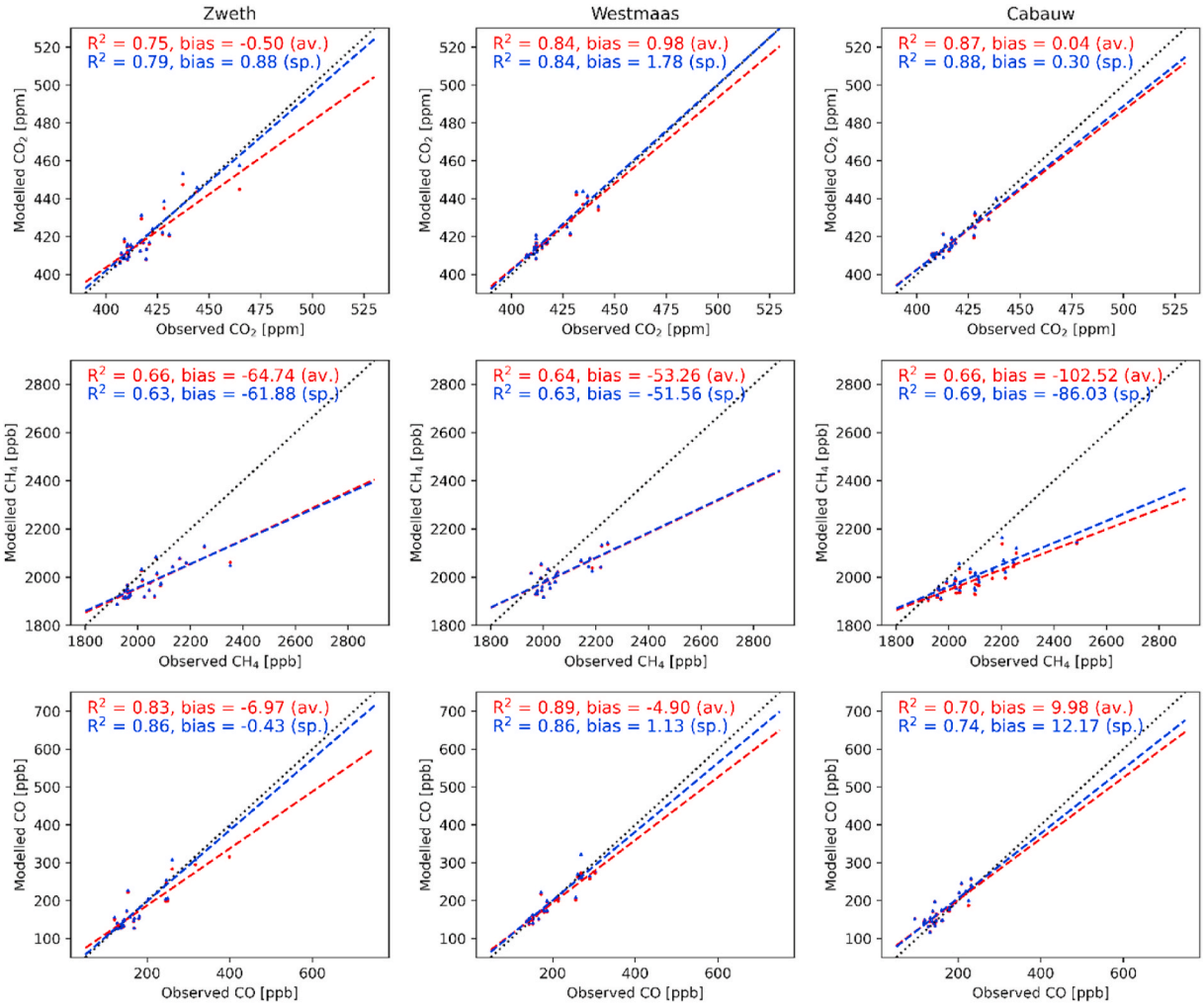

Fig. 9. Scatter plots of daily mean modelled vs. observed CO_2, CH_4 and CO mixing ratios at the three measurement sites. Shown are the model simulations with average (red) and specific (blue) TPs. The black dotted line represents the 1:1 line. Statistics are provided for the comparison between the two model simulations and the observations (av. = average, sp. = specific). (For interpretation of the references to colour in this figure legend, the reader is referred to the Web version of this article.)

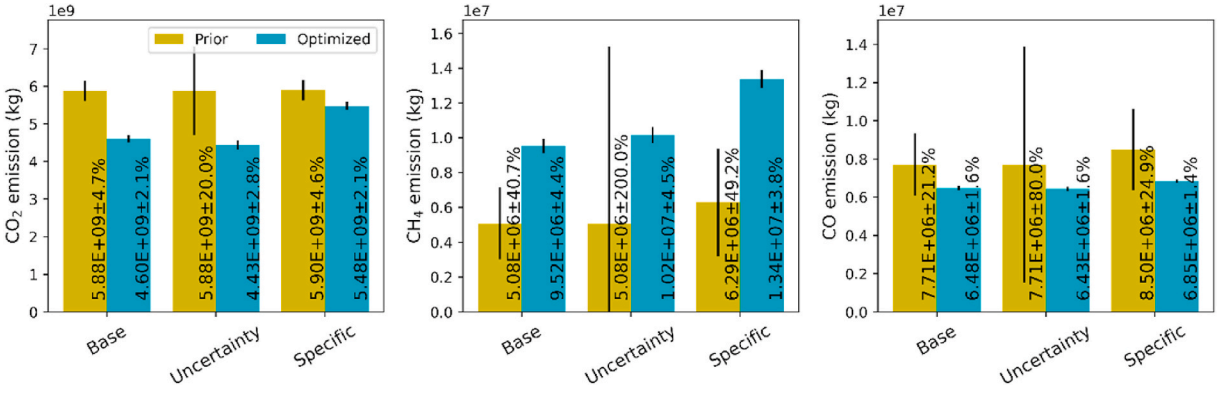

Fig. 10. Prior and optimized monthly emissions of CO_2, CH_4 and CO for the three experiments. Given are the emissions and their 1σ uncertainty, which is also represented by the error bars.

experiment are much closer to the prior. This gives confidence that the specific TPs improve the comparison between the model and observations despite starting with the same overall emissions for January as the 'Base' experiment. Although we expect this conclusion to be valid for CH_4 and CO as well, it partly remains speculation due to the large uncertainty in the annual emissions and in the spatial distribution.

For CH_4 the difference between the 'Average TP' and 'Specific TP' cases is very large. Whereas the CH_4 emissions from agriculture-livestock in January were set to zero in the average TP, the temporal scaling factor for that same sector is 0.7 in the specific TP. This means an

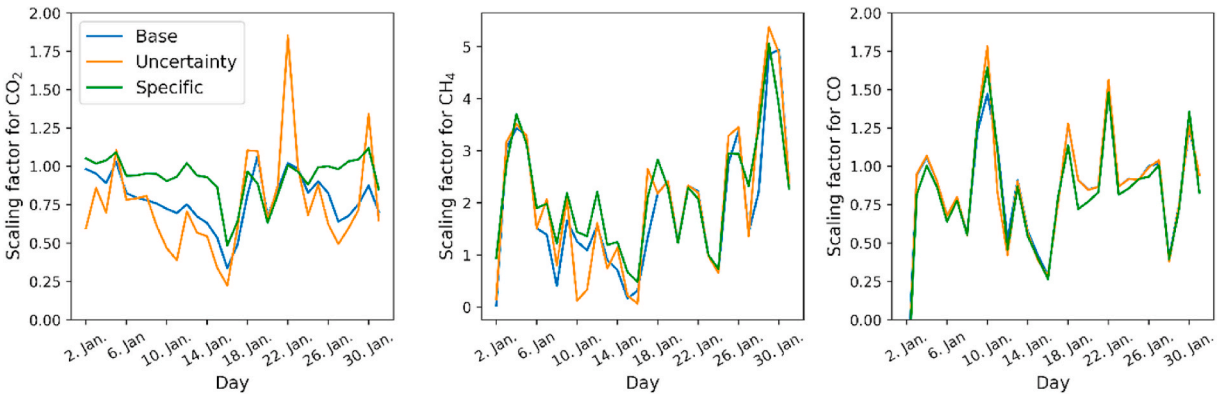

Fig. 11. Daily scaling factors for CO_2, CH_4 and CO emissions for the three experiments.

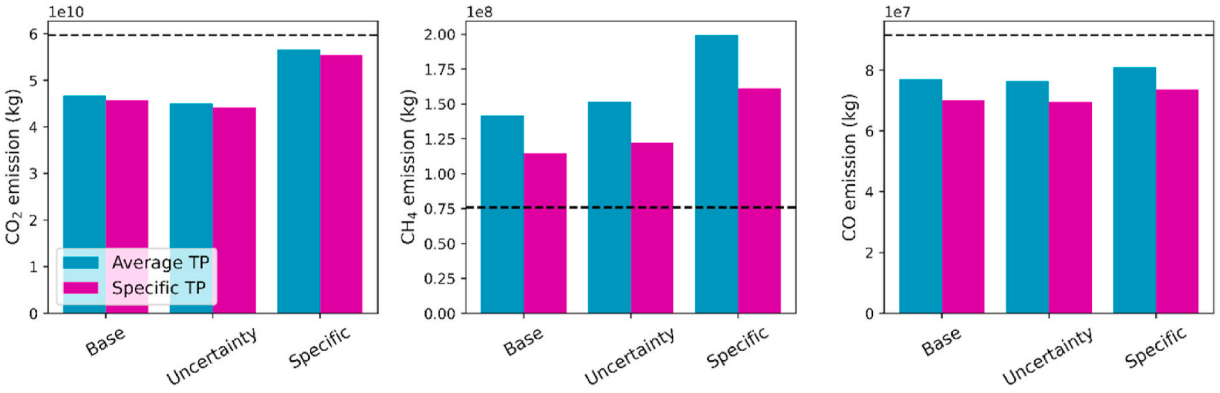

Fig. 12. Yearly emissions of CO_2, CH_4 and CO based on extrapolation of monthly optimized emissions for the three experiments. The extrapolation is done using both average TPs and specific TPs for all experiments, irrespective of their prior TPs. The dashed line indicates the prior yearly emissions taken from the TNO emission inventory.

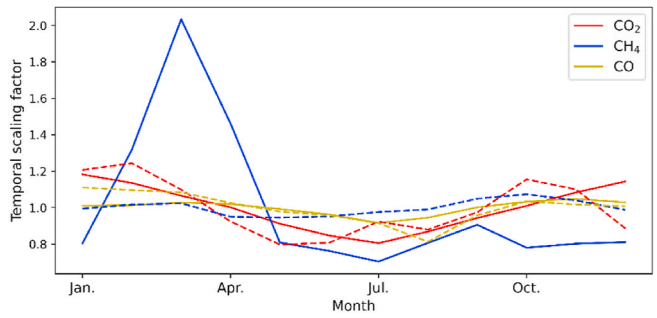

Fig. 13. Monthly variations in emissions of CO_2, CH_4 and CO based on average (full lines) and specific (dashed lines) TPs.

overall temporal scaling factor of 0.8 (average) and 1.0 (specific) in January. In other words, a 20% difference occurs using the two sets of TPs starting from the same prior monthly emission estimate. We also see that the total annual emissions using the original set of TPs (average for 'Base' and specific for 'Specific') for the extrapolation are much closer together than when the opposite TPs (specific for 'Base' and average for 'Specific') are used.

4. Discussion

This paper aims to quantify the impact of various specifications of the temporal variability on the optimization of urban anthropogenic emissions on a monthly time scale. First, a new set of TPs was developed based on actual activity data. We find that the average TPs often used in modelling exercises underestimate variability in the actual activity data. This is due to the use of long-term average data to create average TPs. The specific TPs represent the variability much better compared to the actual activity data. However, we choose to update the TPs for a few source sectors only, based on the availability of high-resolution activity data. Although with the selected source sectors we cover a significant part of the CO_2 (75%) and CO (75%) emissions and about half of the CH_4 emissions (46%), there are several other important sectors that are more challenging to improve. Specifically for CH_4 the TPs for agricultural sectors should receive more attention to ensure the variability in emissions is resolved.

The impact of the various TPs on the simulated mixing ratios is small, even though the small changes appear to be important in the inversions. Previous studies have shown similar results. For example, the impact of different TPs for road transport on the average concentrations of NO_2, O_3 and PM_{10} was shown to be limited, although diurnal peaks and nighttime concentrations were slightly improved (Menut et al., 2012). The simulated mixing ratios in Fig. 9 also show some differences in the day-to-day variability, although this is not necessarily reflected in improved statistics. In addition, small (but important) increases in correlations for hourly and daily mixing ratios of NO_2, SO_2 and PM_{10} were shown as a result of updating the TPs of the same source sectors as in this study (Mues et al., 2014).

This suggests that a large part of the uncertainty in the mixing ratios, and inherently the model-data mismatch, is the result of errors in atmospheric transport and source contributions. Previous studies have looked into different causes of uncertainty (atmospheric transport, prior spatial distribution, prior temporal distribution, uncertain boundary conditions, different inversion schemes) and their relative impact

(Brophy et al., 2019; Feng et al., 2019; Göckede et al., 2010; Hedelius et al., 2018; Martin et al., 2019). Yet there is no consensus as to which factors are the most important due to the differences between studies in spatial and temporal resolutions and the chosen perturbations for each of these factors. Moreover, these studies mostly focused on CO_2, for which the prior emissions are relatively well-known. For CH_4 or CO the uncertainties in the prior (including the TPs) could be larger, making it a more important source of uncertainty. In this study, we show that the TPs do affect the inversions significantly through different pathways. The total prior emissions can change, but also the comparison between the model and observations is affected by the TPs. Overall, we find that the impact of prior uncertainties is smaller than the impact of the different TPs, although a relatively small prior uncertainty increases the importance of having location- and time-specific TPs.

We also examined the impact of TPs on the extrapolation of emission estimates based on short-term campaigns or daytime data to annual emission estimates. Although we find that the annual estimate for CO_2 is closer to the relatively well-known prior when specific TPs are used, we are unable to validate the experiments with observations. Especially for CO and CH_4 we would recommend to invest in an additional observation site to independently validate the experiments. For now, we limit the discussion to the impact of using different TPs. The differences between the two sets of TPs differs per month and therefore the impact on the extrapolation does as well. The maximum difference is 26% for CO_2 (December), which is very large compared to the uncertainty in annual emissions (generally a few percent at country-level). For CH_4 the maximum difference is 101% (March) and for CO 13% (August). This illustrates that an accurate representation of the temporal variability in emissions from different source sectors is important to put the results from a measurement campaign into a broader perspective. Inversions that use daytime data may face similar challenges, because the diurnal cycle in emissions is highly uncertain. We found a difference of 5% (CO_2), 1% (CO) and 36% (CH_4) in the monthly emission estimates using only daytime data compared to the data selection based on wind speed for the 'Base' experiment (not shown). A previous study also showed that using afternoon data to constrain daily emissions can cause an error, because the diurnal cycle is not corrected (Kunik et al., 2019). Additionally, Martin et al. (2019) argued that mixing ratios are often overestimated at night and underestimated during the afternoon, so using daytime data can result in a biased emission estimate that cannot easily be extrapolated to cover an entire year.

The conclusions drawn from this work are not only valid for small spatiotemporal scales. Although larger (regional) scale inversions often cover longer time periods that may cancel out random errors, the change in the source-receptor relationship will sustain and cause a systematic error. The reason for this is that the atmospheric concentrations are correlated with synoptic conditions, both through atmospheric transport and through the impact of the weather on emissions. This effect was previous illustrated by Hendriks et al. (2015), who studied the impact of temporal profiles on air pollutant concentrations from the energy sector, taking into account weather dependencies in renewable energy supply. They concluded that the effect of emission reductions due to renewable energy was smaller when accounting for the impact of synoptic meteorological conditions.

Since the goal of this study was not to actually constrain the monthly or yearly emissions within our study domain we used a relatively simple model set-up. However, several scholars showed a significant spread in the mean optimized emissions when using different correlation length scales (Breón et al., 2015; Kunik et al., 2019). Moreover, Kunik et al. (2019) showed that including temporal error correlations avoids the underestimation of the posterior uncertainty. Another concern is the bias in the CH_4 large-scale background in our forward simulations. We decided to correct for this bias to avoid incorrectly attributing it to local emission sources, which could have had a large impact on the results. For example, Göckede et al. (2010) showed that a shift in advected background CO_2 mixing ratios of 1–2 ppm could cause an error of more than 40% in the biospheric CO_2 flux in the state of Oregon, US. Although we do not know what causes this bias we believe our conclusions are valid because no correction has been applied to CO_2 and CO. Further examination of the bias is needed to use this system for actual emission verification.

Based on our findings we conclude that short-term campaigns can be suited to constrain fossil fuel emissions from cities or specific sources in support of reporting obligations, as was already illustrated by several studies (e.g. (Cui et al., 2017; Gourdji et al., 2018; Wecht et al., 2014)). However, there are a few conditions that need to be met. First of all, it is important to cover not just the afternoon with the measurement campaigns. A focus on the afternoon makes it impossible to constrain the diurnal cycle in emission strengths, which in turn causes a bias in the emission estimate when the diurnal cycle is not correctly described by the TPs. Second, the prior emission inventory should be complete; all sources should be included, even if they are highly uncertain. Missing emissions cannot be scaled and can significantly affect (short-term) inversions. Third, an effort has to be made to improve the description of the temporal variability in emissions to correctly extrapolate the emission estimates to an annual scale.

The final condition, improving the TPs, is gaining increasing attention, but still large steps have to be made towards true location- and time-specific TPs (Matthias et al., 2018). Preferably, TPs should be dependent on location, fuel type and species. We have already shown that the TPs for power plants and road transport are highly dependent on the fuel type, but the road transport emissions of CO are also affected by cold starts (Andrews et al., 2004). Moreover, the degree day method could be applied to each grid cell in the model instead of being based on country-average temperature data, especially for large countries with a strong temperature gradient. Efforts to make such improvements are currently ongoing through the development of dynamic emission models. More detailed emission data can be provided from bottom-up techniques, e.g. using near real-time traffic data (Tu et al., 2018), but this can be computationally expensive and requires a lot of data. Another approach is to use available data to look for typical patterns that can be applied over larger areas or periods of time. Examples could be typical driving behaviour on a roundabout or the prediction that on a sunny weekend day there is additional traffic towards the beach. Note that atmospheric transport models are currently suited to use average TPs applied to annual emissions. Therefore, using detailed emission data requires adaptations to those models as well, either through providing more input data (takes more time) or by online emission processing (less dynamic) (Jähn et al., 2020).

5. Conclusions

We illustrate the impact of using location- and time-specific TPs on the optimization of urban emissions of CO_2, CH_4 and CO. The specific TPs show more variability than the average TPs and are more in line with actual activity data. The impact of specific TPs on the prior emission uncertainty is relatively small, but does not necessarily show a decrease. The reason is that, due to the different TPs, a source sector with a higher uncertainty can become dominant. Nevertheless, both the monthly optimized emissions and the extrapolation to annual emissions are strongly affected by the TPs, causing differences of up to 100% for CH_4. We also find that the TPs affect the source-receptor relationship that influences the direct comparison of observations and models. This results in a 19% higher optimized CO_2 emission using specific TPs, even though the prior monthly emissions were the same with both sets of TPs. We therefore conclude that more effort is needed to improve the representation of the temporal variability in emissions in order to get reliable emission estimates for urban areas using short-term inversions.

Funding

This work was funded by the Netherlands Organisation for Applied

Scientific Research (TNO) through the ERP Climate & Air Quality project.

CRediT authorship contribution statement

Ingrid Super: Conceptualization, Methodology, Writing – original draft, Investigation, Visualization. **Stijn N.C. Dellaert:** Investigation, Writing – review & editing. **Janot P. Tokaya:** Investigation, Writing – review & editing. **Martijn Schaap:** Conceptualization, Investigation, Writing – review & editing.

Declaration of competing interest

The authors declare that they have no known competing financial interests or personal relationships that could have appeared to influence the work reported in this paper.

Acknowledgements

We acknowledge Jean-Matthieu Haussaire (EMPA) for providing the COSMO meteorological input, Julia Marshall (MPI-BGC) for the VPRM runs and Anna Agusti-Panareda (ECMWF) for the C-IFS data. All these input data for the LOTOS-EUROS model simulations have been developed under the CHE Horizon 2020 project. We also thank Arjo Segers (TNO) for helping with the set-up of LOTOS-EUROS and Marcel Moerman and Arnoud Frumau (TNO) for ensuring the continuity of the observations. Finally, the observational data used in this publication is generated by the Ruisdael Observatory, a scientific infrastructure financed by the Dutch Research Council (NWO).

References

Andres, R.J., Boden, T.A., Higdon, D.M., 2016. Gridded uncertainty in fossil fuel carbon dioxide emission maps, a CDIAC example. Atmos. Chem. Phys. 16, 14979–14995. https://doi.org/10.5194/acp-16-14979-2016.

Andrews, G.E., Zhu, G., Li, H., Simpson, A., Wylie, J.A., Bell, M., Tate, J., 2004. The Effect of Ambient Temperature on Cold Start Urban Traffic Emissions for a Real World SI Car. SAE 2004 Powertrain Fluid Syst. https://doi.org/10.4271/2004-01-2903.

Baldauf, M., Seifert, A., Förstner, J., Majewski, D., Raschendorfer, M., Reinhardt, T., 2011. Operational convective-scale numerical weather prediction with the COSMO model: description and sensitivities. Mon. Weather Rev. 139, 3887–3905. https://doi.org/10.1175/MWR-D-10-05013.1.

Bergamaschi, P., Danila, A., Weiss, R.F., Ciais, P., Thompson, R.L., Brunner, D., Levin, I., Meijer, Y., Chevallier, F., Janssens-Maenhout, G., Bovensmann, H., Crisp, D., Basu, S., Dlugokencky, E., Engelen, R., Gerbig, C., Günther, D., Hammer, S., Henne, S., Houweling, S., Karstens, U., Kort, E.A., Maione, M., Manning, A.J., Miller, J., Montzka, S., Pandey, S., Peters, W., Peylin, P., Pinty, B., Ramonet, M., Reimann, S., Röckmann, T., Schmidt, M., Strogies, M., Sussams, J., Tarasova, O., Van Aardenne, J., Vermeulen, A.T., Vogel, F., 2018. Atmospheric Monitoring and Inverse Modelling for Verification of Greenhouse Gas Inventories. Publications Office of the European Union, Luxembourg. https://doi.org/10.2760/759928.

Boon, A., Broquet, G., Clifford, D.J., Chevallier, F., Butterfield, D.M., Pison, I., Ramonet, M., Paris, J.D., Ciais, P., 2016. Analysis of the potential of near-ground measurements of CO2 and CH4 in London, UK, for the monitoring of city-scale emissions using an atmospheric transport model. Atmos. Chem. Phys. 16, 6735–6756. https://doi.org/10.5194/acp-16-6735-2016.

Breón, F.M., Broquet, G., Puygrenier, V., Chevallier, F., Xueref-Remy, I., Ramonet, M., Dieudonné, E., Lopez, M., Schmidt, M., Perrussel, O., Ciais, P., 2015. An attempt at estimating Paris area CO2 emissions from atmospheric concentration measurements. Atmos. Chem. Phys. 15, 1707–1724. https://doi.org/10.5194/acp-15-1707-2015.

Brophy, K., Graven, H., Manning, A.J., White, E., Arnold, T., Fischer, M.L., Jeong, S., Cui, X., Rigby, M., 2019. Characterizing uncertainties in atmospheric inversions of fossil fuel CO2 emissions in California. Atmos. Chem. Phys. 19, 2991–3006. https://doi.org/10.5194/acp-19-2991-2019.

Ciais, P., Rayner, P., Chevallier, F., Bousquet, P., Logan, M., Peylin, P., Ramonet, M., 2010. Atmospheric inversions for estimating CO2 fluxes: methods and perspectives. Climatic Change 103, 69–92. https://doi.org/10.1007/s10584-010-9909-3.

Cui, Y.Y., Brioude, J., Angevine, W.M., Peischl, J., McKeen, S.A., Kim, S., Neuman, J.A., Henze, D.K., Bousserez, N., Fischer, M.L., Jeong, S., Michelsen, H.A., Bambha, R.P., Liu, Z., Santoni, G.W., Daube, B.C., Kort, E.A., Frost, G.J., Ryerson, T.B., Wofsy, S.C., Trainer, M., 2017. Top-down estimate of methane emissions in California using a mesoscale inverse modeling technique: the San Joaquin Valley. J. Geophys. Res. Atmos. 122, 3686–3699. https://doi.org/10.1002/2016JD026398.

Curier, R.L., Timmermans, R., Calabretta-Jongen, S., Eskes, H., Segers, A., Swart, D., Schaap, M., 2012. Improving ozone forecasts over Europe by synergistic use of the LOTOS-EUROS chemical transport model and in-situ measurements. Atmos. Environ. 60, 217–226. https://doi.org/10.1016/j.atmosenv.2012.06.017.

Denier van der Gon, H.A.C., Hendriks, C., Kuenen, J., Segers, A., Visschedijk, A., 2011. Description of Current Temporal Emission Patterns and Sensitivity of Predicted AQ for Temporal Emission Patterns. TNO, Utrecht, Netherlands [online] Available from. https://atmosphere.copernicus.eu/sites/default/files/2019-07/MACC_TNO_del_1_3_v2.pdf.

Feng, S., Lauvaux, T., Keller, K., Davis, K.J., Rayner, P., Oda, T., Gurney, K.R., 2019. A road map for improving the treatment of uncertainties in high-resolution regional carbon flux inverse estimates. Geophys. Res. Lett. 46, 13461–13469. https://doi.org/10.1029/2019GL082987.

Frumau, A., Hensen, A., Vermeulen, A., ICOS Atmosphere Thematic Centre, 2020. Drought-2018 CO2 molar fraction product from Cabauw (1.0) [Data set]. ICOS Carbon Portal. https://doi.org/10.18160/EJEX-W9BF.

Ganesan, A.L., Manning, A.J., Grant, A., Young, D., Oram, D.E., Sturges, W.T., Moncrieff, J.B., O'Doherty, S., 2015. Quantifying methane and nitrous oxide emissions from the UK and Ireland using a national-scale monitoring network. Atmos. Chem. Phys. 15, 6393–6406. https://doi.org/10.5194/acp-15-6393-2015.

Gately, C.K., Hutyra, L.R., 2017. Large uncertainties in urban-scale carbon emissions. J. Geophys. Res. Atmos. 122, 242–260. https://doi.org/10.1002/2017JD027359.

Göckede, M., Turner, D.P., Michalak, A.M., Vickers, D., Law, B.E., 2010. Sensitivity of a subregional scale atmospheric inverse CO2 modeling framework to boundary conditions. J. Geophys. Res. Atmos. 115, D24112 https://doi.org/10.1029/2010JD014443.

Gourdji, S.M., Yadav, V., Karion, A., Mueller, K.L., Conley, S., Ryerson, T., Nehrkorn, T., Kort, E.A., 2018. Reducing errors in aircraft atmospheric inversion estimates of point-source emissions: the Aliso Canyon natural gas leak as a natural tracer experiment. Environ. Res. Lett. 13, 045003 https://doi.org/10.1088/1748-9326/aab049.

Graven, H., Fischer, M.L., Lueker, T., Jeong, S., Guilderson, T.P., Keeling, R.F., Bambha, R., Brophy, K., Callahan, W., Cui, X., Frankenberg, C., Gurney, K.R., Lafranchi, B.W., Lehman, S.J., Michelsen, H., Miller, J.B., Newman, S., Paplawsky, W., Parazoo, N.C., Sloop, C., Walker, S.J., 2018. Assessing fossil fuel CO2 emissions in California using atmospheric observations and models. Environ. Res. Lett. 13, 065007 https://doi.org/10.1088/1748-9326/aabd43.

Guevara, M., Jorba, O., Soret, A., Petetin, H., Bowdalo, D., Serradell, K., Tena, C., Denier van der Gon, H., Kuenen, J., Peuch, V.H., Pérez Garciá-Pando, C., 2021. Time-resolved emission reductions for atmospheric chemistry modelling in Europe during the COVID-19 lockdowns. Atmos. Chem. Phys. 21, 773–797. https://doi.org/10.5194/acp-21-773-2021.

Hedelius, J.K., Liu, J., Oda, T., Maksyutov, S., Roehl, C.M., Iraci, L.T., Podolske, J.R., Hillyard, P.W., Liang, J., Gurney, K.R., Wunch, D., Wennberg, P.O., 2018. Southern California megacity CO2, CH4, and CO flux estimates using ground-and space-based remote sensing and a Lagrangian model. Atmos. Chem. Phys. 18, 16271–16291. https://doi.org/10.5194/acp-18-16271-2018.

Hendriks, C., Kuenen, J., Kranenburg, R., Scholz, Y., Schaap, M., 2015. A shift in emission time profiles of fossil fuel combustion due to energy transitions impacts source receptor matrices for air quality. Environ. Sci. Process. Impacts 17, 510–524. https://doi.org/10.1039/C4EM00444B.

Hutchins, M.G., Colby, J.D., Marland, G., Marland, E., 2017. A comparison of five high-resolution spatially-explicit, fossil-fuel, carbon dioxide emission inventories for the United States. Mitig. Adapt. Strat. Gl. 22, 947–972. https://doi.org/10.1007/s11027-016-9709-9.

IEA, 2008. World Energy Outlook 2008, Paris [online] Available from. https://www.iea.org/reports/world-energy-outlook-2008.

Jähn, M., Kuhlmann, G., Mu, Q., Haussaire, J.M., Ochsner, D., Osterried, K., Clément, V., Brunner, D., 2020. An online emission module for atmospheric chemistry transport models: implementation in COSMO-GHG v5.6a and COSMO-ART v5.1-3.1, Geosci. Model Dev 13, 2379–2392. https://doi.org/10.5194/gmd-13-2379-2020.

Kort, E.A., Angevine, W.M., Duren, R., Miller, C.E., 2013. Surface observations for monitoring urban fossil fuel CO2 emissions: minimum site location requirements for the Los Angeles megacity. J. Geophys. Res. Atmos. 118, 1–8. https://doi.org/10.1002/jgrd.50135.

Kranenburg, R., Segers, A.J., Hendriks, C., Schaap, M., 2013. Source apportionment using LOTOS-EUROS: module description and evaluation. Geosci. Model Dev. (GMD) 6, 721–733. https://doi.org/10.5194/gmd-6-721-2013.

Kunik, L., Mallia, D.V., Gurney, K.R., Mendoza, D.L., Oda, T., Lin, J.C., 2019. Bayesian inverse estimation of urban CO2 emissions: results from a synthetic data simulation over Salt Lake City, UT. Elem. Sci. Anth. 7 https://doi.org/10.1525/elementa.375.

Lauvaux, T., Miles, N.L., Richardson, S.J., Deng, A., Stauffer, D.R., Davis, K.J., Jacobson, G., Rella, C., Calonder, G.P., Decola, P.L., 2013. Urban emissions of CO2 from Davos, Switzerland: the first real-time monitoring system using an atmospheric inversion technique. J. Appl. Meteorol. Climatol. 52, 2654–2668. https://doi.org/10.1175/JAMC-D-13-038.1.

Lauvaux, T., Miles, N.L., Deng, A., Richardson, S.J., Cambaliza, M.O., Davis, K.J., Gaudet, B., Gurney, K.R., Huang, J., O'Keefe, D., Song, Y., Karion, A., Oda, T., Patarasuk, R., Razlivanov, I., Sarmiento, D., Shepson, P., Sweeney, C., Turnbull, J., Wu, K., 2016. High-resolution atmospheric inversion of urban CO2 emissions during the dormant season of the Indianapolis Flux Experiment (INFLUX). J. Geophys. Res. Atmos. 121, 5213–5236. https://doi.org/10.1002/2015JD024473.

Liander, 2020. Datadiensten: Open Data [online] Available from. https://www.liander.nl/partners/datadiensten/open-data/data. (Accessed 20 June 2020).

Mahadevan, P., Wofsy, S.C., Matross, D.M., Xiao, X., Dunn, A.L., Lin, J.C., Gerbig, C., Munger, J.W., Chow, V.Y., Gottlieb, E.W., 2008. A satellite-based biosphere parameterization for net ecosystem CO2 exchange: Vegetation Photosynthesis and

Respiration Model (VPRM). Global Biogeochem. Cycles 22, GB2005. https://doi.org/10.1029/2006GB002735.

Manders, A.M.M., Builtjes, P.J.H., Curier, L., Denier van der Gon, H.A.C., Hendriks, C., Jonkers, S., Kranenburg, R., Kuenen, J.J.P., Segers, A.J., Timmermans, R.M.A., Visschedijk, A.J.H., Wichink Kruit, R.J., Van Pul, W.A.J., Sauter, F.J., Van der Swaluw, E., Swart, D.P.J., Douros, J., Eskes, H., Van Meijgaard, E., Van Ulft, B., Van Velthoven, P., Banzhaf, S., Mues, A.C., Stern, R., Fu, G., Lu, S., Heemink, A., Van Velzen, N., Schaap, M., 2017. Curriculum vitae of the LOTOS – EUROS (v2.0) chemistry transport model. Geosci. Model Dev. (GMD) 10, 4145–4173. https://doi.org/10.5194/gmd-10-4145-2017.

Martin, C.R., Zeng, N., Karion, A., Mueller, K., Ghosh, S., Lopez-Coto, I., Gurney, K.R., Oda, T., Prasad, K., Liu, Y., Dickerson, R.R., Whetstone, J., 2019. Investigating sources of variability and error in simulations of carbon dioxide in an urban region. Atmos. Environ. 199, 55–69. https://doi.org/10.1016/j.atmosenv.2018.11.013.

Matthias, V., Arndt, J.A., Aulinger, A., Bieser, J., Denier van der Gon, H., Kranenburg, R., Kuenen, J., Neumann, D., Pouliot, G., Quante, M., 2018. Modeling emissions for three-dimensional atmospheric chemistry transport models. J. Air Waste Manag. Assoc. 68, 763–800. https://doi.org/10.1080/10962247.2018.1424057.

Menut, L., Goussebaile, A., Bessagnet, B., Khvorostiyanov, D., Ung, A., 2012. Impact of realistic hourly emissions profiles on air pollutants concentrations modelled with CHIMERE. Atmos. Environ. 49, 233–244. https://doi.org/10.1016/j.atmosenv.2011.11.057.

Mues, A., Manders, A., Schaap, M., Van Ulft, L.H., Van Meijgaard, E., Builtjes, P., 2013. Differences in particulate matter concentrations between urban and rural regions under current and changing climate conditions. Atmos. Environ. 80, 232–247. https://doi.org/10.1016/j.atmosenv.2013.07.049.

Mues, A., Kuenen, J., Hendriks, C., Manders, A., Segers, A., Scholz, Y., Hueglin, C., Builtjes, P., Schaap, M., 2014. Sensitivity of air pollution simulations with LOTOS-EUROS to the temporal distribution of anthropogenic emissions. Atmos. Chem. Phys. 14, 939–955. https://doi.org/10.5194/acp-14-939-2014.

Nathan, B.J., Lauvaux, T., Turnbull, J.C., Richardson, S.J., Miles, N.L., Gurney, K.R., 2018. Source sector attribution of CO2 emissions using an urban CO/CO2 Bayesian inversion system. J. Geophys. Res. Atmos. 123, 13611–13621. https://doi.org/10.1029/2018JD029231.

Peylin, P., Houweling, S., Krol, M.C., Karstens, U., Rödenbeck, C., Geels, C., Vermeulen, A., Badawy, B., Aulagnier, C., Pregger, T., Delage, F., Pieterse, G., Ciais, P., Heimann, M., 2011. Importance of fossil fuel emission uncertainties over Europe for CO2 modeling: model intercomparison. Atmos. Chem. Phys. 11, 6607–6622. https://doi.org/10.5194/acp-11-6607-2011.

Sauter, F., Van Zanten, M., Van der Swaluw, E., Aben, J., De Leeuw, F., Van Jaarsveld, H., 2016. The OPS-Model. Description of OPS 4.5.0. Bilthoven. [online] Available from. https://www.rivm.nl/media/ops/v4.5.0/OPS-model-v4.5.0.pdf.

Staufer, J., Broquet, G., Bréon, F.M., Puygrenier, V., Chevallier, F., Xueref-Rémy, I., Dieudonné, E., Lopez, M., Schmidt, M., Ramonet, M., Perrussel, O., Lac, C., Wu, L., Ciais, P., 2016. The first 1-year-long estimate of the Paris region fossil fuel CO2 emissions based on atmospheric inversion. Atmos. Chem. Phys. 16, 14703–14726. https://doi.org/10.5194/acp-16-14703-2016.

Super, I., Denier van der Gon, H.A.C., Visschedijk, A.J.H., Moerman, M.M., Chen, H., van der Molen, M.K., Peters, W., 2017. Interpreting continuous in-situ observations of carbon dioxide and carbon monoxide in the urban port area of Rotterdam. Atmos. Pollut. Res. 8, 174–187. https://doi.org/10.1016/j.apr.2016.08.008.

Super, I., Denier Van Der Gon, H.A.C., Van Der Molen, M.K., Dellaert, S.N.C., Peters, W., 2020a. Optimizing a dynamic fossil fuel CO2 emission model with CTDAS (CarbonTracker Data Assimilation Shell, v1.0) for an urban area using atmospheric observations of CO2, CO, NOx, and SO2, Geosci. Model Dev 13, 2695–2721. https://doi.org/10.5194/gmd-13-2695-2020.

Super, I., Dellaert, S.N.C., Visschedijk, A.J.H., Van Der Gon, H.A.C.D., 2020b. Uncertainty analysis of a European high-resolution emission inventory of CO2 and CO to support inverse modelling and network design. Atmos. Chem. Phys. 20, 1795–1816. https://doi.org/10.5194/acp-20-1795-2020.

Tu, R., Kamel, I., Wang, A., Abdulhai, B., Hatzopoulou, M., 2018. Development of a hybrid modelling approach for the generation of an urban on-road transportation emission inventory. Transport. Res. Transport Environ. 62, 604–618. https://doi.org/10.1016/j.trd.2018.04.011.

Turnbull, J.C., Sweeney, C., Karion, A., Newberger, T., Lehman, S.J., Tans, P.P., Davis, K.J., Lauvaux, T., Miles, N.L., Richardson, S.J., Cambaliza, M.O., Shepson, P.B., Gurney, K., Patarasuk, R., Razlivanov, I., 2015. Toward quantification and source sector identification of fossil fuel CO2 emissions from an urban area: results from the INFLUX experiment. J. Geophys. Res. Atmos. 120, 292–312. https://doi.org/10.1002/2013JD020225.

UNFCCC, 2015. Paris Agreement, UNFCCC [online] Available from. http://unfccc.int/files/essential_background/convention/application/pdf/english_paris_agreement.pdf.

UNFCCC, 2020. National Inventory Submissions 2020 [online] Available from. https://unfccc.int/process-and-meetings/transparency-and-reporting/reporting-and-review-under-the-convention/greenhouse-gas-inventories-annex-i-parties/national-inventory-submissions-2020. (Accessed 20 June 2020).

Van der Laan, S., Manohar, S., Vermeulen, A., Bosveld, F., Meijer, H., Manning, A., Van der Molen, M., Van der Laan-Luijkx, I., 2016. Inferring 222Rn soil fluxes from ambient 222Rn activity and eddy covariance measurements of CO2. Atmos. Meas. Tech. 9, 5523–5533. https://doi.org/10.5194/amt-9-5523-2016.

Van Der Laan-Luijkx, I.T., Van Der Velde, I.R., Van Der Veen, E., Tsuruta, A., Stanislawska, K., Babenhauserheide, A., Fang Zhang, H., Liu, Y., He, W., Chen, H., Masarie, K.A., Krol, M.C., Peters, W., 2017. The CarbonTracker data assimilation shell (CTDAS) v1.0: implementation and global carbon balance 2001-2015, geosci. Model Dev 10, 2785–2800. https://doi.org/10.5194/gmd-10-2785-2017.

Van Jaarsveld, J.A., 2004. The Operational Priority Substances Model. Description and Validation of OPS-Pro 4.1. Bilthoven, Netherlands. [online] Available from. https://www.pbl.nl/sites/default/files/downloads/500045001.pdf.

Vermeulen, A.T., Hensen, A., Popa, M.E., Van Den Bulk, W.C.M., Jongejan, P.A.C., 2011. Greenhouse gas observations from Cabauw tall tower (1992-2010). Atmos. Meas. Tech. 4, 617–644. https://doi.org/10.5194/amt-4-617-2011.

Vogel, F.R., Thiruchittampalam, B., Theloke, J., Kretschmer, R., Gerbig, C., Hammer, S., Levin, I., 2013. Can we evaluate a fine-grained emission model using high-resolution atmospheric transport modelling and regional fossil fuel CO2 observations? Tellus B Chem. Phys. Meteorol. 65 https://doi.org/10.3402/tellusb.v65i0.18681 1.

Ware, J., Kort, E.A., Duren, R., Mueller, K.L., Verhulst, K., Yadav, V., 2019. Detecting urban emissions changes and events with a near-real-time-capable inversion system. J. Geophys. Res. Atmos. 124, 5117–5130. https://doi.org/10.1029/2018JD029224.

Wecht, K.J., Jacob, D.J., Sulprizio, M.P., Santoni, G.W., Wofsy, S.C., Parker, R., Bösch, H., Worden, J., 2014. Spatially resolving methane emissions in California: constraints from the CalNex aircraft campaign and from present (GOSAT, TES) and future (TROPOMI, geostationary) satellite observations. Atmos. Chem. Phys. 14, 8173–8184. https://doi.org/10.5194/acp-14-8173-2014.

Whitaker, J.S., Hamill, T.M., 2002. Ensemble data assimilation without perturbed observations. Mon. Weather Rev. 130, 1913–1924. https://doi.org/10.1175/152010.1175/1520-0493(2002)130<1913:EDAWPO>2.0.CO;2.